Journal of Physical Science, Vol. 34(1), 27–41, 2023

Photodegradation of Oxytetracycline Using Fluorescent Light Driven ZnO Quantum Dots Synthesised Via Microwave Method

Normawati Jasni,[1] Anwar Iqbal,[1*] Noor Hana Hanif Abu Bakar,[1] W. Maryam Wan Hazman Danial,[3] M.W. Ismail[3] and Kalaivizhi Rajappan[4]

[1]School of Chemical Sciences, Universiti Sains Malaysia, 11800 Gelugor, Penang, Malaysia
[2]School of Physics, Universiti Sains Malaysia, 11800 Gelugor, Penang, Malaysia
[3]Department of Chemistry, Kulliyyah of Science, International Islamic University Malaysia, 25200 Kuantan, Pahang, Malaysia
[4]Department of Chemistry, SRM Institute of Science and Technology, Kattankulathur, Chengalpattu 603203, India

[*]Corresponding author: anwariqbal@usm.my

Published online: 28 April 2023

To cite this article: Jasni, N. et al. (2023). Photodegradation of oxytetracycline using fluorescent light driven ZnO quantum dots synthesised via microwave method. *J. Phys. Sci.*, 34(1), 27–42. https://doi.org/10.21315/jps2023.34.1.3

To link to this article: https://doi.org/10.21315/jps2023.34.1.3

ABSTRACT: *In this study, Li^+ ions capped zinc oxide quantum dots (ZnO QDs) was synthesised using the microwave method. The X-ray diffraction (XRD), transmission electron microscopy (TEM), high-transmission electron microscopy (HR-TEM), scanning electron microscopy (SEM), UV–Visible diffuse reflectance spectroscopy (UV-DRS), and photoluminescence (PL) techniques were used to characterise the structural, morphological, optical properties of the ZnO QDs. The XRD analysis reveals that ZnO QDs have a hexagonal wurtzite structure with an average crystallite size of 9.9 nm. The morphology of ZnO QDs was observed to be quasi-spherically shaped with an average particle size of 10 nm. The PL analysis detected the presence of various defects. All these factors enhanced the photodegradation of oxytetracycline (OTC) under fluorescent light irradiation. Within 40 min, 88.3% of OTC was removed, which was higher compared to the bulk ZnO reported in the literature. This technology is aimed at small animal husbandries due to the photocatalyst synthesis method's simplicity and the photocatalysis process's requirements.*

Keywords: ZnO QDs, quantum dots, photocatalysis, oxytetracycline, microwave method

1. INTRODUCTION

Each year, over 200 000 tonnes of antibiotics are produced to treat various bacterial infections in humans and agriculture.[1] Oxytetracycline (OTC) is a wide-spectrum antibiotic used to treat gram-positive and gram-negative bacteria-related diseases. The OTC is chemically stable because of its polyaromatic ring structure.[2] It has been discovered in water, soil and food in parts per billion (ppb) to parts per million (ppm) concentrations.[3,4] The presence of OTC in the natural environment is concerning since it can induce the growth of antibiotic-resistant bacteria and jeopardise ecosystem stability.[5] This condition is worsened because conventional wastewater treatment facilities could not effectively remove the OTC. The photocatalytic method is a green chemical technology that utilises light irritation and photocatalysts to generate powerful reactive oxygen species (ROS) such as hydroxyl radicals ($^{\bullet}OH$) and superoxide radical ($O_2^{\bullet-}$) to mineralised organic pollutants.

Zinc oxide (ZnO) is a wide band gap (E_g = 3.37 eV) semiconductor, non-toxic, affordable, extremely photosensitive, and photocatalytically active.[6] It has a more positive valence band position than other semiconductor materials (about 3.00 eV vs. NHE), which suggests that it has a stronger ability to excite holes in light and is better suited for the oxidative destruction of organic pollutants. However, it is highly effective under UV light irradiation. Additionally, its photocatalytic uses are constrained by the high rate of recombination of photogenerated electron/hole (e^-/h^+) pairs.[7–9]

Quantum dots (QDs) are semiconductor nanocrystals that have small emission spectra, excellent photochemical stability, and sustained absorption spectra.[10] Due to these photophysical properties, QDs have the potential to be applied in photocatalysis. Additionally, the surface defects on QDs also function as electron scavengers, slowing the recombination rate of the e^-/h^+ pairs and making them excellent electron acceptors.[11] Hence, ZnO quantum dots (ZnO QDs) will demonstrate better photodegradation activity than bulk ZnO.

This paper demonstrates the synthesis of ZnO QDs via the microwave synthesis method utilising Li^+ ions as the capping agent. The ZnO QDs' photocatalytic capability was investigated in the oxytetracycline (OTC) degradation process under fluorescent light irradiation. The addition of Li^+ ions reduced the size and enhanced the photocatalytic of the ZnO QDs by creating various defects.

2. EXPERIMENTAL

2.1 Synthesis of ZnO QDs

The ZnO QDs were synthesised according to Asok et al., with some modifications.[12] The lithium hydroxide, LiOH (99%, anhydrous, QRC chemicals, United Kingdom), (1 mmol) was dissolved in 20 ml of ethanol (99.5%, HmBEG chemical, Malaysia) and stirred for 30 min at room temperature (Solution A). The zinc acetate dihydrate, $Zn(CH_3COO)_2.2H_2O$ (98%, QRC chemicals, Malaysia), (1.0 mmol) was stirred in 20 ml of ethanol for 30 min at room temperature (Solution B). Solution A was added slowly to solution B and continuously stirred for another 30 min. The mixture was irradiated with a domestic microwave oven (SAMSUNG/MODEL No: MW61F, Malaysia) for 6 min at 100 W. White powder was isolated from the mother liquor by centrifugation after the mixture was cooled to room temperature, filtered, and repeatedly washed with ethanol to get rid of unreacted reactants. The sample was dried for 24 h at 50°C in an oven for 24 h.

2.2 Characterisation of ZnO QDs

The surface of the ZnO QDs was studied using scanning electron microscopy (SEM, Quanta FEG-650, United Kingdom) and high-transmission electron microscopy on a TECNAI G2 20 S-TWIN, FEI with an acceleration voltage of 200 kV, United States). The crystal structure and size of ZnO QDs were measured using an x-ray powder diffractometer (Bruker D8 Advance, Germany) by using monochromatic Cu Ka radiation (λ = 0.15406 nm). Diffraction data ranged from 20°–80° and 0.02°/min scanning speed. The crystallite sizes of ZnO QDs were calculated using the Debye-Scherrer formula:

$$D = \frac{0.9\lambda}{\beta \cos \theta} \quad (1)$$

where D is the average crystallite size (nm), λ is the x-ray wavelength (= 0.15406 nm), β is the peak's full width at half-maximum (FWHM), and the θ is the Bragg angle. Photoluminescence (PL) measurements were confirmed using Perkin Elmer LS-55, United States spectroscopy at room temperature, which was measured with a Xenon lamp (325 nm) as the exciton source. The photo-absorption and band gap energy (E_g) were measured using UV-DRS (a Perkin Elmer Lambda 35 UV/Vis spectrometer, United States). X-ray photoelectron spectroscopy (XPS) analysis was performed using AXIS Ultra DLD, Kratos, United Kingdom. The Al Kα (1486.6 eV) was used as the x-ray source, and the binding energy was referenced to an adventitious carbon at 284.6 eV.

2.3 Photodegradation of oxytetracycline (OTC)

The photodegradation of OTC was conducted in a homemade reactor (Figure 1) attached with two fluorescent lights (each 24 W). The light intensity was determined to be 104 W/m^2 with a 0.40 W/m^2 residual UV leakage irradiance using a Dual-Input Data Logging Radiometer (Model PMA 100, Pennsylvania, United States). The photodegradation of OTC (95%, Acros organic, United States) as a pollutant model was carried out as follows: photocatalyst (10 mg) was added into 50 ml of OTC solution (10 mg/l, pH = 9) and agitated in the dark for 20 min before to irradiation to reach an adsorption-desorption equilibrium. Samples were collected every 10 min after the irradiation started and filtered with a 0.22 µm membrane filter and measured using the UV-2600, Shimadzu (Japan) spectrometer. The OTC removal efficiency was calculated using the formula below:

$$\text{OTC degradation (\%R)} = \frac{C_0 - C_t}{C_0} \times 100 \qquad (2)$$

where C_o and C_t represent the concentration before light irradiation and concentration at a time interval (t, min).

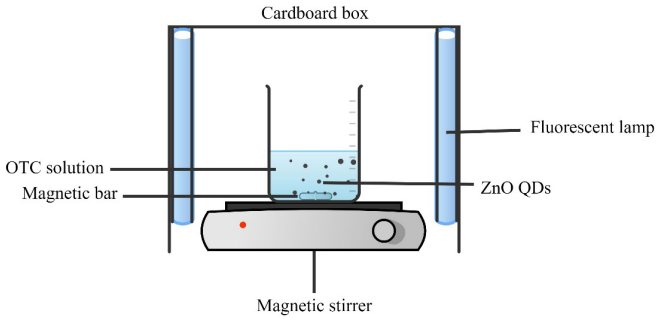

Figure 1: The schematic diagram for a handmade reactor used in the photodegradation of OTC.

3. RESULTS AND DISCUSSION

3.1 X-ray Diffraction (XRD) Analysis

The XRD diffractogram peaks of the ZnO QDs is shown in Figure 2(a). The diffractogram pattern is similar to the hexagonal wurtzite structure of ZnO (JCPDS card: 36-1451).[13] The diffraction peaks at $2\theta = 31.80^o$, 34.42^o and 36.28^o are assigned to the *hkl* planes of (100), (002) and (101), respectively. Diffraction

peaks related to Li^+ ions are not detected. Therefore, it is concluded that the Li^+ ions could possibly be substituted within the lattice of ZnO. This is possible since the radius of Zn (0.74 Å) is smaller than the radius of Li (0.76 Å).[14] The broadening of the diffraction peaks compared to typical ZnO indicates that the addition of Li^+ ion deformed the ZnO QDs crystal lattice and produced crystallites with smaller sizes.[15,16] The synthesised ZnO QDs are considered to be pure since diffraction peaks related to other chemical constituents were not detected.[15] The average diameter of the ZnO QDs crystallite is 9.9 nm.

3.2 Morphology Study

The SEM image shown in Figure 2(b) indicate that ZnO QDs are quasi-spherically shaped. Spherically shaped structures are reported to be better photocatalysts due to the wider surface.[17] The TEM image [Figure 2(c)] also indicates the presence of quasi-spherically shaped nanoparticles with some aggregation. The average particle size of ZnO QDs determined from measuring over 100 particles using ImageJ software was approximately 10.0 nm 0.39 nm. The particle size histogram is given as an insert in Figure 2(c).[16] The ZnO QDs were found to have a lattice spacing of 0.26 nm and 0.28 nm, which closely matched the crystal structure of the wurtzite phases of ZnO (002) and (100).[18]

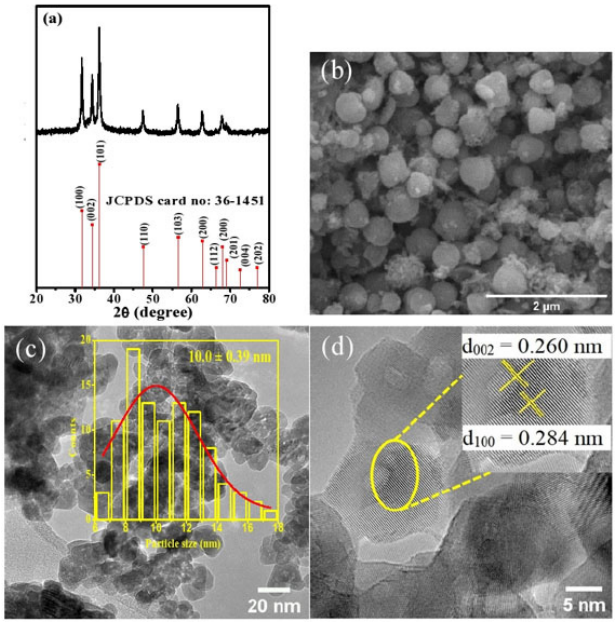

Figure 2: The (a) XRD, (b) SEM, (c) TEM and (d) HRTEM image of ZnO QDs. The particle size histogram is given as the inset in Figure 2(c).

3.3 Optical Absorption

From the UV-DRS absorption spectrum of the ZnO QDs [Figure 3(a)], it can be observed that the ZnO QDs show good absorption of incident light in the range of 350 nm–400 nm, which belongs to the ultraviolet (UV) region.[15] The partial absorption edge in the ZnO QDs is seen to be extended into the visible domain.[19] These observations indicate that the synthesised ZnO QDs have a good absorption range in both UV and visible regions. The E_g was determined using the Tauc method. The E_g is given in the inset of Figure 2(a). The E_g of the ZnO QDs (3.21 eV) was lower than that of bulk ZnO (3.37 eV).[20] It has been demonstrated that ZnO QDs can absorb lower energy photons, as a result, can take part in the photodegradation process with a greater number of photogenerated e^-/h^+. This suggests that the photodegradation of ZnO QDs is expected to be improved.[15] The increase in network disorder brought on by Li^+'s introduction into the network can be attributed to the band gap narrowing. The disorderness produced continuous defects close to the band edges, which is shown by the standard bond length and angle in the crystal.[21]

3.4 Photoluminescence Study

The deconvolution of the PL spectrum [Figure 3(b)] resulted in several Gaussian components. The peak in the ultraviolet region, specifically at 400 nm is generally attributed to the free-exciton recombination of ZnO, which is called near band edge (NBE) emission.[22] The second emission peak in the violet-blue region (~440 nm) is attributed to the Zn interstitial (Zn_i) defect due to the charge transfer process from the metal ion to the defect centres. When the photogenerated carriers recombine from Zn_i to Zn vacancy (V_{Zn}) energy states, then emission in the blue (470 nm) appears.[23] The fourth emission peak at 531 nm causes the green emission peak resulting from the oxygen vacancy (V_O) created by integrating Li ions into the ZnO crystal lattice. The Li-ions cannot substitute for O (LiO) in the crystal lattice due to their high formation energy, but they can diffuse into the spaces between the lattices as interstitials (Li_i), in addition to being substitutional.[24–27]

3.5 X-ray photoelectron spectroscopy (XPS)

As shown in the wide scan XPS spectrum [Figure 3(c)], Zn, O, C and Li were detected on the surface of ZnO QDs. The peak related to Li is not prominent due to its lower concentration. Only a single peak at 55 eV was observed in the high-resolution XPS spectrum of Li 1s [Figure 3(d)]. The peak is attributed to the Li at substitutional (Li_{Zn}) sites and indicates Li_{Zn}-O bonds' formation.[28] The binding energy (BE) of Li is similar to that reported by Song et al., and Ravichandran et al.[29,30] The element C originated from the adventitious carbon used in the calibration

of binding energies. Zn, O, C and Li atomic concentrations were 40.32%, 51.72%, 7.24% and 0.11%, respectively.

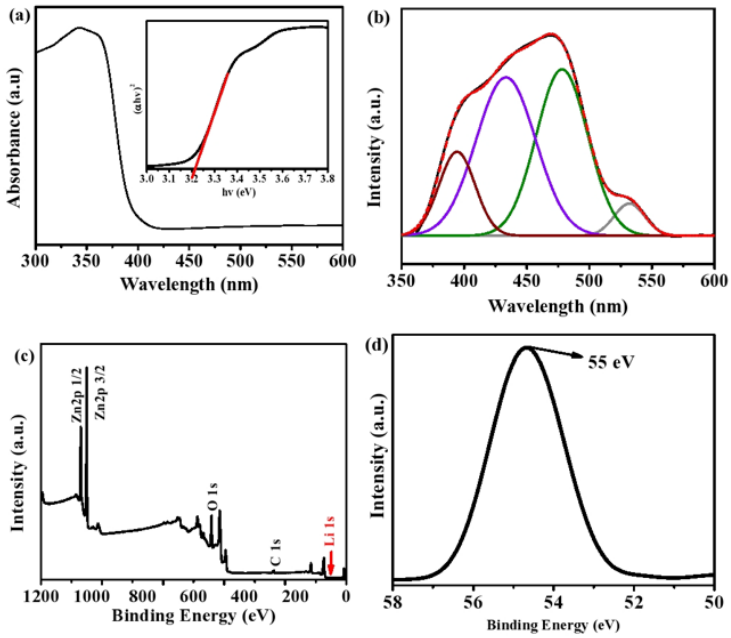

Figure 3: (a) The UV-vis diffuse reflectance spectra with estimated band gap (insert), (b) deconvoluted PL spectrum, (c) wide XPS spectrum and (d) high-resolution Li 1s XPS spectrum of ZnO QDs.

3.6 Photodegradation of OTC

Figure 4 (a) shows the OTC reduction over time. The kinetic curves are plotted [Figure 4 (b)] and calculated using the following equation:

$$-in\left(\frac{C_t}{C_0}\right) = kt \tag{3}$$

where C_o (mg/l) represents the initial OTC before irradiation, C_t (mg/l) is the OTC concentration at a given time, and k (min^{-1}) is the reaction rate.

Based on Figure 4 (a), without the presence of any photocatalysts (photolysis), the removal percentage of OTC was only 14.8%. The OTC's naphthacene ring is chemically stable and will not decompose effectively.[31] The removal of OTC due to adsorption was determined to be 48.9%. When the light was switched on, the removal of OTC increased to 88.3%. Hence, the contribution from photocatalysis

is 39.4%. Thus it is concluded that the removal of OTC by ZnO QDs is driven by adsorption and photocatalysis. The removal of OTC has an excellent linear relationship and approaches a pseudo-first-order reaction [Figure 4 (b)]. The resulting reaction rate of the ZnO QDs was calculated to be 0.04453 min^{-1}. The characteristic absorption band of OTC centred at 357 nm was observed to decrease as time progressed, implying successful photodegradation.

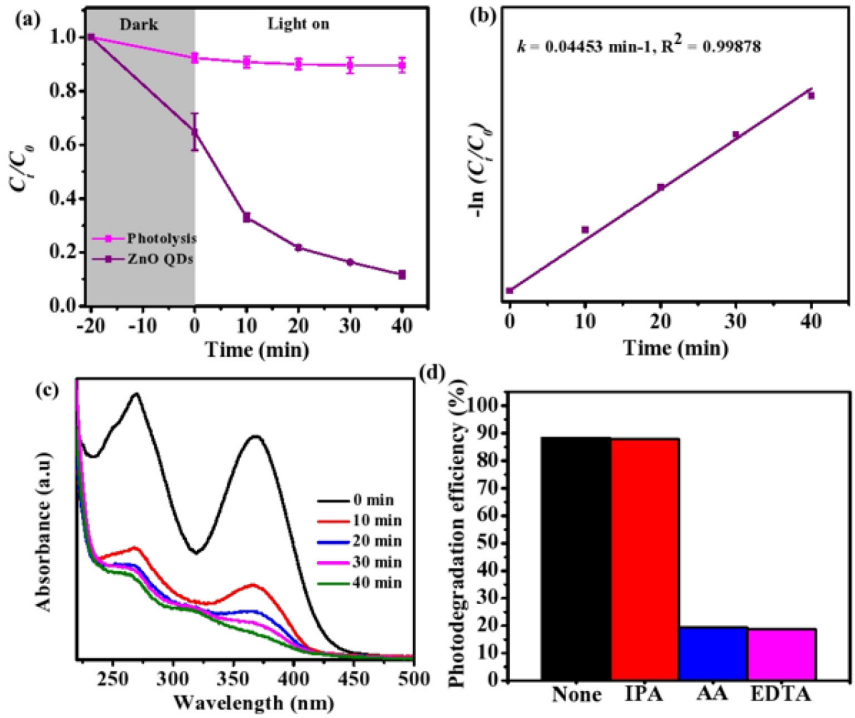

Figure 4: The (a) OTC removal profile, (b) rate constant of ZnO QDs in the photodegradation of OTC, (c) time-dependence absorption spectra of OTC and (d) effect of scavengers on photodegradation of OTC.

The removal percentage of OTC using the ZnO QDs was also compared with bulk ZnO-based photocatalysts reported in the literature (Table 1). The removal percentage of OTC was lower, and the photocatalysts required a longer reaction time and high light intensity. Even though sunlight is low cost and can give better removal, it hardly ever has constant light intensity.

Table 1: Comparison of the photocatalytic efficiency of OTC degradation for different ZnO photocatalyst.

Catalyst	Reaction condition	Removal (%)	k (min^{-1})	Ref.
ZnO/ZrO_2	[OTC] = 10 mg/l, Dosage = 24000 mg/l, Light source = Spectroline XX 15N UV lamp Duration = 120 min	60	0.0079	34
ZnO NPs	[OTC] = 10 mg/l, Dosage = 1000 mg/l, Light source = 400W Halogen lamp, Time = 300 min	68	0.00299	35
Cu doped ZnO-MWCNT	[OTC] = 50 mg/l, Dosage = 500 mg/l, Light source = 400W Halogen lamp, Duration = 240 min	55	0.021	36
$ZnO/ZnFe_2O_4$/ diatomite	[OTC] = 10 mg/l, Dosage = 1000 mg/l, Light source = 300W Xenon lamp, Duration =150 min	95	0.0098	37
ZnO-TiO_2 nanohybrids	[OTC] = 60 mg/l, Dosage = 1000 mg/l, Light source = Sunlight (Intensity 862 W/cm^2), Duration = 8 min	90.3	0.2740	38
Fe-Ni/ZnO	[OTC] = 20 mg/l, Dosage = 600 mg/l, Light source = 300W Xenon lamp, Duration= 120 min	87.9	0.014	39
ZnO-Bentonite	[OTC] = 20 mg/l, Dosage = 4000 mg/l, Light source = a series of six Philips UV lamps 20 W, Duration = 120 min	87	0.0173	40
ZnO QDs	[OTC] = 10 mg/l, Dosage = 200 g/l, Light source = 48W two compact fluorescent lamp, Time = 40 min	88.3	0.04453	This work

The enhanced photodegradation activity of ZnO QDs is attributed to the quantum confinement effect (QCE) and the crystal defects in the ZnO QDs lattice caused by the addition of Li^+ ions. Due to the restricted electron movement, a wide band gap is produced, rapidly preventing recombination processes that would otherwise result in the loss of active electrons.[32] The crystal defects enhance photodegradation by reducing the rate at which the photogenerated e^-/h^+ pairs recombination.[33] By reducing the rate, more ROS can be created to mineralise the OTC. The ZnO QDs have wider surfaces than those offered by spherically arranged structures, which exhibit higher adsorption capacities. Whereas reduction of its band gap can reflect and absorb the incident light more often and maximise photon utilisation, resulting in a significant increase in the degradation activity and requirement for high-intensity light source.

Scavenging tests were performed to identify the generated (ROS). Ascorbic acid (AA), isopropyl alcohol (IPA), and ethylenediaminetetraacetic acid (EDTA) were utilised as scavenging agents for , •OH, and h^+, respectively. Figure 4(d) displays the impact of several scavengers on photodegradation. The OTC percentage reduced significantly to 19.4% and 18.6%, respectively, when AA and EDTA was added. Hence, it is concluded that and h^+ plays the most crucial role in the photodegradation of OTC.

Understanding the band edge properties of ZnO QDs is important in establishing the photodegradation mechanism. The following formulas are used to determine the valence band (VB) and conduction band (CB) edges:

$$E_{VB} = X - E_e + 0.5E_g \quad (4)$$

$$E_{CB} = E_{VB} - E_g \quad (5)$$

where E_g and E_e are the photocatalyst's band gap and electron energy on the hydrogen scale, respectively (4.5 eV). Whereas X is 5.79 eV for ZnO's electronegativity. The calculated E_g value of ZnO QDs is 3.21 eV. The E_{CB} and E_{VB} were –0.32 eV (in V vs. NHE) and 2.895 eV. Under light irradiation, electrons (e^-) will be exited from the CB to the VB leaving holes (h^+) in the CB. Since the E_{CB} potential edge is more negative compared to the redox potential of $O_2/O_2^{\bullet-}$ (–0.046 eV vs. NHE), the e^- are capable of reducing the adsorbed O_2 on the photocatalyst to $O_2^{\bullet-}$. [41] The E_{VB} value of ZnO QDs is higher than the potential of H_2O/•OH (+2.2 eV vs. NHE scale). Hence, the h^+ can oxidise the H_2O to •OH, which in turn oxidises OTC.[42] Meanwhile, the •OH can also originate from the interaction of $O_2^{\bullet-}$. with H_2O molecules.[43] The final decomposition and destruction of OTC is accomplished by the decomposition of active •OH, $O_2^{\bullet-}$, and h^+ and eventually break it down into

CO_2 and H_2O. The possible reaction mechanism for the photodegradation of OTC is shown in Figure 5.

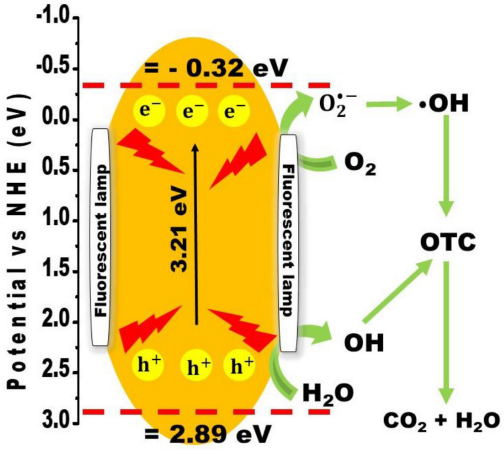

Figure 5: Possible charge transmission mechanism of photodegradation of OTC using ZnO QDs.

4. CONCLUSION

In this study, ZnO QDs were successfully synthesised using the microwave method with Li^+ ions as capping agents for the photodegradation of OTC under fluorescent illumination. The percent removal of OTC (88.3%) was higher than other reported bulk ZnO (Table 1) and required less time and lower light intensity. The increased photocatalytic activity of the ZnO QDs corresponds to the quantum confinement effect and crystal defects from adding Li^+ ions. Due to the simplicity of the synthesis method, requirements for effective photocatalysis to take place, and maintenance, this technology is suitable for use in small animal husbandries.

5. ACKNOWLEDGEMENTS

The authors are thankful to the Malaysian Ministry of Education (Higher Education) for the Fundamental Research Grant Scheme (FRGS/1/2019/STG01/USM/02/7) to support this research.

6. REFERENCES

1. Wu, J. et al. (2022). NiCo/ZnO/g-C_3N_4 Z-scheme heterojunction nanoparticles with enhanced photocatalytic degradation oxytetracycline. *Diam. Relat. Mater.*, 121, 108738. https://doi.org/10.1016/j.diamond.2021.108738
2. Yan, W. et al. (2018). The changes of bacterial communities and antibiotic resistance genes in microbial fuel cells during long-term oxytetracycline processing. *Water Res.*, 142, 105–114. https://doi.org/10.1016/j.watres.2018.05.047
3. Gu, J. et al. (2018). Surface tension driven aggregation of organic nanowires via lab in a droplet. *Nanoscale*, 10(23), 11006–11012. https://doi.org/10.1039/c8nr02592d
4. Ren, X. et al. (2017). Toxic responses of swimming crab (Portunus trituberculatus) larvae exposed to environmentally realistic concentrations of oxytetracycline. *Chemosphere*, 173, 563–571. https://doi.org/10.1016/j.chemosphere.2017.01.078
5. Senasu, T. et al. (2021). Sunlight-driven photodegradation of oxytetracycline antibiotic by $BiVO_4$ photocatalyst. *J. Solid State Chem.*, 297, 122088. https://doi.org/10.1016/j.jssc.2021.122088
6. Yasin, M. et al. (2022). Development of Bi_2O_3-ZnO heterostructure for enhanced photodegradation of rhodamine B and reactive yellow dyes. *Surf. Interfaces*, 30, 101846. https://doi.org/10.1016/j.surfin.2022.101846
7. Wang, A. et al. (2022). MOF-derived N-doped ZnO carbon skeleton@hierarchical Bi_2MoO_6 S-scheme heterojunction for photodegradation of SMX: Mechanism, pathways and DFT calculation. *J. Hazard. Mater.*, 426, 128106. https://doi.org/10.1016/j.jhazmat.2021.128106
8. Ullattil, S. G. et al. (2016). Self-Doped ZnO Microrods—High Temperature Stable Oxygen Deficient Platforms for Solar Photocatalysis. *Ind. Eng. Chem. Res.*, 55(22), 6413–6421. https://doi.org/10.1021/acs.iecr.6b01030
9. An, M. et al. (2022). CdS QDs modified three-dimensional ordered hollow spherical $ZnTiO_3$-ZnO-TiO_2 composite with improved photocatalytic performance. *J. Alloys Compd.*, 895, 162638. https://doi.org/10.1016/j.jallcom.2021.162638
10. Jr, M. B. et al. (1998). Semiconductor nanocrystals as fluorescent biological labels. *SCIENCE*, 281 (5385), 2013–2016. https://doi.org/10.1126/science.281.5385.2013
11. Dutra, L. V. et al. (2022). Green synthesis optimisation of graphene quantum dots by Doehlert design for dye photodegradation application. *Colloids Surf. A: Physicochem. Eng. Asp.*, 651, 129442. https://doi.org/10.1016/j.colsurfa.2022.129442

12. Asok, A. et al. (2013). Microwave accelerated one-minute synthesis of luminescent ZnO quantum dots. *AIP Conference Proceedings*, 1512(1). 404–405. https://doi.org//10.1063/1.4791082
13. Mohamed, W. A. A. et al. (2020). Zinc oxide quantum dots for textile dyes and real industrial wastewater treatment: Solar photocatalytic activity, photoluminescence properties and recycling process. *Adv. Powder Technol.*, 31(6), 2555–2565. https://doi.org/10.1016/j.apt.2020.04.017
14. Meziane, K. et al. (2017). Li concentration dependence of structural properties and optical band gap of Li-doped ZnO films. *Appl. Phys. A.*, 123(6), 430. https://doi.org/10.1007/s00339-017-1039-6
15. Gao, X. et al. (2022). ZnO QDs and three-dimensional ordered macroporous structure synergistically enhance the photocatalytic degradation and hydrogen evolution performance of WO_3/TiO_2 composites. *J. Phys. Chem. Solids*, 165, 110655. https://doi.org/10.1016/j.jpcs.2022.110655
16. Chen, L. et al. (2022). Facile synthesis of MoS_2/ZnO quantum dots for enhanced visible-light photocatalytic performance and antibacterial applications. *Nano-Struc. Nano-Objects*, 30, 100873. https://doi.org/10.1016/j.nanoso.2022.100873
17. Alberti, S. et al. (2021). Experimental and physico-chemical comparison of ZnO nanoparticles' activity for photocatalytic applications in wastewater treatment. *Catalysts*, 11(6), 678. https://doi.org/10.3390/catal11060678
18. Zou, T. et al. (2020). Water-soluble ZnO quantum dots modified by (3-aminopropyl) triethoxysilane: The promising fluorescent probe for the selective detection of Cu^{2+} ion in drinking water. *J. Alloys Compds.*, 825, 153904. https://doi.org/10.1016/j.jallcom.2020.153904
19. Hsieh, M. L. et al. (2022). Synthesis and characterisation of high-performance ZnO/graphene quantum dot composites for photocatalytic degradation of metronidazole. *J. Taiwan Inst. Chem. Eng.*, 131, 104180. https://doi.org/10.1016/j.jtice.2021.104180
20. Mishra, S. M., & Satpati, B. (2022). Morphology of ZnO nanorods and Au–ZnO heterostructures on different seed layers and their influence on the optical behavior. *J. Lumin.*, 246, 118813. https://doi.org/10.1016/j.jlumin.2022.118813
21. Hjiri, M. et al. (2019). Study of defects in Li-doped ZnO thin films. *Mater. Sci. Semicond. Process.*, 89, 149–153. https://doi.org/10.1016/j.mssp.2018.09.010
22. Vempati, S. et al. (2012). One-step synthesis of ZnO nanosheets: A blue-white fluorophore. *Nanoscale Res. Lett.*, 7(1), 470. https://doi.org/10.1186/1556-276x-7-470
23. Dash, D. et al. (2022). Nanocrystalline gadolinium doped ZnO: An excellent photoluminescent material and efficient photocatalyst towards optoelectronic and environment remedial applications. *Ceram. Int*., 48(19), 139. https://doi.org/10.1016/j.ceramint.2022.03.139
24. Panigrahy, B. et al. (2010). Defect-related emissions and magnetisation properties of ZnO nanorods. *Adv. Funct. Mater.,* 20(7), 1161–1165. https://doi.org/10.1002/adfm.200902018

25. Vanheusden, K. et al. (1996). A. Correlation between photoluminescence and oxygen vacancies in ZnO phosphors. *App. Phys. Lett.*, 68(3), 403–405. https://doi.org/10.1063/1.116699
26. Wardle, M. G. et al. (2005). Theory of Li in ZnO: A limitation for Li-based p-type doping. *Phys. Rev. B.*, 71(15), 155205. https://doi.org/10.1103/PhysRevB.71.155205
27. Ruankham, P. et al. (2011). Vertically aligned ZnO nanorods doped with lithium for polymer solar cells: defect related photovoltaic properties. *J. Mater. Chem.*, 21(26), 9710–9715. https://doi.org/10.1039/c0jm04452k
28. Awan, S et al. (2012). Ferromagnetism in Li doped ZnO nanoparticles: The role of interstitial Li. *J. Appl. Phys.*, 112(10), 103924. https://doi.org/10.1063/1.4767364
29. Song, X. et al. (2017). High-efficiency and low-cost Li/ZnO catalysts for synthesis of glycerol carbonate from glycerol transesterification: The role of Li and ZnO interaction. *Appl. Catal. A-Gen.*, 532, 77–85. https://doi.org/10.1016/j.apcata.2016.12.019
30. Ravichandran, C. et al. (2010). Investigations on the structural and optical properties of Li, N and (Li, N) co-doped ZnO thin films prepared by sol–gel technique. *Mater. Sci. Semicond. Process.*, 13(1), 46–50. https://doi.org/10.1016/j.mssp.2010.02.006
31. Zheng, L. et al. (2022). Synergistically enhanced oxygen reduction reaction and oxytetracycline mineralisation by FeCoO/GO modified cathode in microbial fuel cell. *Sci. Total Environ.*, 808, 151873. https://doi.org/10.1016/j.scitotenv.2021.151873
32. Bajorowicz, B. et al. (2018). Quantum dot-decorated semiconductor micro- and nanoparticles: A review of their synthesis, characterisation and application in photocatalysis. *Adv. Colloid Interface Sci.*, 256, 352–372. https://doi.org/10.1016/j.cis.2018.02.003
33. Tong, S. et al. (2022). Preparation of carbon quantum dots/TiO_2 composite and application for enhanced photodegradation of rhodamine B. *Colloids Surf. A: Physicochem. Eng. Asp*., 648, 129342. https://doi.org/10.1016/j.colsurfa.2022.129342
34. Vaizoğullar, A. I. (2019). ZnO/ZrO_2 composites: Synthesis characterisation and photocatalytic performance in the degradation of oxytetracycline antibiotic. *Mater. Technol.*, 34(8), 433–443. https://doi.org/10.1080/10667857.2019.1574287
35. Falamas, A. et al. (2022). Size-dependent spectroscopic insight into the steady-state and time-resolved optical properties of ZnO photocatalysts. *Mater. Sci. Semicond. Process.*, 145, 106644. https://doi.org/10.1016/j.mssp.2022.106644
36. Toloman, D. et al. (2021). Visible-light-driven photocatalytic degradation of different organic pollutants using Cu doped ZnO-MWCNT nanocomposites. *J. Alloys Compd.*, 866, 159010. https://doi.org/10.1016/j.jallcom.2021.159010
37. Xue, L. et al. (2022). Fabrication of magnetic ZnO/$ZnFe_2O_4$/diatomite composites: improved photocatalytic efficiency under visible light irradiation. *J. Mater. Sci.: Mater. Electron.*, 33(3), 1405–1424. https://doi.org/10.1007/s10854-021-07568-w

38. Singh, J. et al. (2020). Fabrication of ZnO–TiO_2 nanohybrids for rapid sunlight driven photodegradation of textile dyes and antibiotic residue molecules. *Opt. Mater.*, 107, 110338. https://doi.org/10.1016/j.optmat.2020.110138
39. Guo, J., et al. (2014). Preparation of transition-metal-doped ZnO nanophotocatalysts and their performance on photocatalytic degradation of antibiotic wastewater. *Desalination Water Treat.*, 1–8. https://doi.org/10.1080/19443994.2014.961171
40. Vaizoğullar, A. İ. (2018). Comparing photocatalytic activity of ZnO and nanospherical ZnO/bentonite catalyst: Preparation, structural characterization and their photocatalytic performances using oxytetracycline antibiotic in aqueous solution. *J. Mex. Chem. Soc.*, 62(1), 578. https://doi.org/10.29356/jmcs.v62i1.578
41. Shao, B. et al. (2022). Construction of Bi_2WO_6/CoAl-LDHs S-scheme heterojunction with efficient photo-Fenton-like catalytic performance: Experimental and theoretical studies. *Chemosphere*, 291, 133001. https://doi.org/10.1016/j.chemosphere.2021.133001
42. Sharma, A. et al. (2016). Studies on structural defects in bare, PVP capped and TPPO capped copper oxide nanoparticles by positron annihilation lifetime spectroscopy and their impact on photocatalytic degradation of rhodamine B. *RSC Adv.*, 6(78), 74812–74821. https://doi.org/10.1039/c6ra12795a
43. Zhang, S. et al. (2022). Atomic Fe sites embedded within carbon nanotubes for the efficient photodegradation of multiple tetracyclines. *Sep. Purif. Technol.*, 287. https://doi.org/10.1016/j.seppur.2022.120530